Progress In Electromagnetics Research, Vol. 134, 419–435, 2013

AN ITERATIVE SOURCE RECONSTRUCTION METHOD EXPLOITING PHASELESS ELECTRIC FIELD DATA

Ping Li* **and Lijun Jiang**

Department of Electrical and Electronic Engineering, The University of Hong Kong, Hong Kong, China

Abstract—Conventional equivalent source reconstruction methods (SRM) require both phase and amplitude information of the acquired field data. However, there are situations where the phase information is not available or impractical to obtain. Hence, the development of SRM using phaseless fields is important. In this paper, a novel iterative SRM based on phaseless electric fields is presented. The reconstructed equivalent current source can be electric, magnetic current, or both. They can fit the physical geometry of the radiator. Electric field integral equation (EFIE) is employed to build the relationship between the reconstructed current source and measured fields. It can precisely reproduce the original 3D radiation pattern with very good accuracy. To investigate the robustness and accuracy of the proposed approach, both strong and weakly-directional radiators are benchmarked.

1. INTRODUCTION

Followed by the near field data post processing, advanced near field measurement techniques are broadly applied to antenna diagnostics [1], far field (FF) prediction, and radiation pattern synthesis [2–4], etc.. Because the near field (NF) data contains intrinsic information for antenna characterizations [5], the source reconstruction methods (SRM) are employed to recover the near field equivalent sources so that the near field radiation mechanism as well as the far field radiation pattern can be analyzed.

Most SRMs are based on both amplitude and phase measurements of the field. The equivalent sources are of different forms on different near field surfaces calculated from the phase and magnitude measurements of different field components. In [6, 7], the equivalent

Received 21 October 2012, Accepted 28 November 2012, Scheduled 6 December 2012

* Corresponding author: Ping Li (liping@eee.hku.hk).

source is the magnetic current represented by the 2D pulse basis functions on an infinite fictitious perfect electric conductor (PEC) plane in front of the antenna aperture. It is calculated from the measured planar electric field over a near field plane. A similar idea is proposed in [5], in which the equivalent source is a set of planar electric currents over a perfect magnetic conductor (PMC) plane. The PMC plane can be further eliminated via the image theory. Only the radiation pattern in the upper semisphere region toward to the measurement plane can be recovered. In [8, 9], equivalent electric and magnetic current sources are reconstructed over a spherical surface enclosing the antenna or the surface of the antenna itself. The resultant equivalent current source can be used to characterize the full 3D radiation pattern. Some other SRMs have been proposed in [10–16], those based on the approach in [13, 23] have shown to have a higher stability and accuracy [16, 26, 27].

The above-mentioned SRMs work only when both field amplitude and phase are available. However, phase measurement is usually difficulty since the measurement probe is quite sensitive to the surrounding environment and equipment variation. Hence, the SRM based on the amplitude-only data is needed to conduct antenna characterization and NF-FF transformation. In [19], only based on amplitude measurements over a planar surface, the equivalent magnetic current over a PEC near field surface is reconstructed through a direct optimization approach. However, it merely works for the upper semi-spherical region due to its adoption of the planar measurement surface. More importantly, it is only suitable to highly directive radiators. For less directive or omnidirectional radiators, the accuracy of this method is limited. Later, phaseless E-field data is employ for spherical modal expansion [20], where the field outside the expansion spherical surface is reproduced but can not predict the field inside the spherical surface.

In this paper, a novel "iterative SRM" based on the amplitude-only field measurement is presented. Different from the direct optimization methods [19, 21] using the amplitude data over only one measurement surface, the proposed source reconstruction process is implemented in a forward and backward propagating fashion over two different measured spherical surfaces. Hence, the proposed method has more flexibility to reconstruct the source more accurately. Meanwhile the proposed method produces the whole 3D radiation pattern with very good accuracy while the methods in [19, 21] are only effective for strong radiation directions.

The paper is organized as follows: in Section 2, the principle of SRM using both amplitude and phase information is described. In Section 3, the proposed phaseless "iterative SRM" is presented.

In Section 4, numerical verifications are provided. Conclusions and discussions are given at the end of the paper.

2. GENERAL PRINCIPLE OF TRADITIONAL SRM

The electromagnetic equivalence principle [22] states that only the tangential electric or magnetic field over a closed surface surrounding the device/antenna under test (DUT/AUT) is needed to characterize the electromagnetic radiation. The tangential electric and magnetic fields can correspond to the equivalent magnetic and electric currents if the procedure described in [23] is followed. Based on the above principle, the SRM can be facilitated as: given an arbitrary DUT/AUT, bound by a surface S', an equivalent source can be built over this surface, as shown in Fig. 1. This equivalent source may be the electric current $\mathbf{J}_{s'}$, magnetic current $\mathbf{M}_{s'}$ or both as explained in [23]. It can reproduce the original radiation outside that surface. This equivalent source can be determined by the measured field data over arbitrary domain through an inverse process as shown in Fig. 1.

In our method, EFIE is employed since electric field measurement

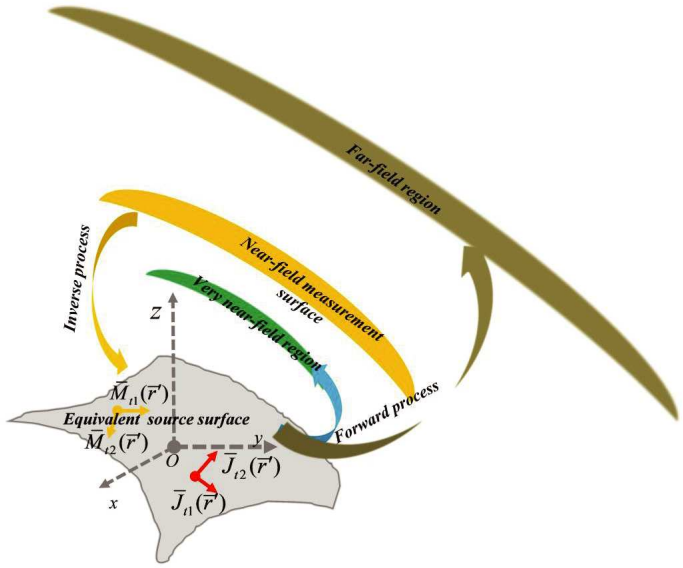

Figure 1. The equivalent source reconstruction process and the NFNF or NF-FF transformation post-processing.

is preferred. The general formula is written as

$$\mathbf{E}(\mathbf{r}_{Meas}) = \mathbf{E}_{\mathbf{J}s'}(\mathbf{r}_{Meas}) + \mathbf{E}_{\mathbf{M}s'}(\mathbf{r}_{Meas}) \tag{1}$$

where $\mathbf{E}$ is the electric field at the measurement position, $\mathbf{E}_{\mathbf{J}_{s'}}$ the electric field radiated by the equivalent current, and $\mathbf{E}_{\mathbf{M}_{s'}}$ the electric field radiated by the equivalent magnetic current. If $\mathbf{r}_{Meas}$ and $\mathbf{r}'$ represent the measurement and source positions, respectively, we have [13, 23]

$$\mathbf{E}_{\mathbf{J}s'}(\mathbf{r}_{Meas}) = -j\eta_0 k_0 \int_{s'} \left[\mathbf{J}_{s'}(\mathbf{r}') + \frac{1}{k_0^2}\nabla\nabla'_s \cdot \mathbf{J}_{s'}(\mathbf{r}')\right] \frac{e^{-jkR}}{4\pi R} dS' \tag{2}$$

$$\mathbf{E}_{\mathbf{M}s'}(\mathbf{r}_{Meas}) = \int_{s'} \mathbf{M}_{s'}(\mathbf{r}') \times \nabla \frac{e^{-jkR}}{4\pi R} dS' \tag{3}$$

where $k_0 = \omega\sqrt{\epsilon_0\mu_0}$ is the free space wave number, $\eta_0 = \sqrt{\frac{\mu_0}{\epsilon_0}}$ the vacuum characteristic wave impedance, and R the distance between the measurement point and source position.

The surface where equivalent currents reside is meshed into non-overlapping triangles. The equivalent currents are expanded by Rao-Wilton-Glisson (RWG) [24] basis functions and expressed as

$$\mathbf{J}_{s'}\left(\mathbf{r}'\right) = J_0 \sum_{n=1}^{N_e} P_n^e \mathbf{J}_n(\mathbf{r}') \tag{4}$$

$$\mathbf{M}_{s'}\left(\mathbf{r}'\right) = M_0 \sum_{m=1}^{N_h} P_n^h \mathbf{J}_m(\mathbf{r}') \tag{5}$$

where J_0 and M_0 are two normalization factors. $\mathbf{J}_n$ denotes the n-th RWG basis function for electric current $\mathbf{J}_{s'}$ and $\mathbf{J}_m$ the m-th RWG basis function for magnetic current $\mathbf{M}_{s'}$, and P_n^e and P_m^h are the corresponding coefficients.

In order to obtain the unknown expansion coefficients in (4) and (5), a vector weighting function is introduced

$$\boldsymbol{\omega}(\mathbf{r}) = \delta(\mathbf{r} - \mathbf{r}_{Meas})\hat{\mathbf{e}}_t \tag{6}$$

where $\delta(\mathbf{r} - \mathbf{r}_{Meas})$ denoting the Kronecker delta function is equal to one at the measurement position. $\hat{\mathbf{e}}_t$ represents polarization directions of the measurement probe. In this paper, we assume that the measurement probe is a linearly polarized antenna and the measurement is along θ and ϕ directions at every measurement point. Thus, polarization vectors $\hat{\mathbf{e}}_t = \hat{\mathbf{e}}_\theta$ or $\hat{\mathbf{e}}_t = \hat{\mathbf{e}}_\phi$.

Substituting (2) and (3) into (1) with (4) and (5), and taking inner products of the integral equation with the weighting function in (6),

the following matrix equations are obtained

$$\begin{pmatrix} \overline{\mathbf{E}}_\theta \\ \overline{\mathbf{E}}_\phi \end{pmatrix} = \begin{pmatrix} \overline{\overline{\mathbf{Z}}}_{\theta,J_{s'}}(\mathbf{e}_\theta, \mathbf{J}_{s'}) & \overline{\overline{\mathbf{Z}}}_{\theta,M_{s'}}(\mathbf{e}_\theta, \mathbf{M}_{s'}) \\ \overline{\overline{\mathbf{Z}}}_{\phi,J_{s'}}(\mathbf{e}_\phi, \mathbf{J}_{s'}) & \overline{\overline{\mathbf{Z}}}_{\phi,M_{s'}}(\mathbf{e}_\phi, \mathbf{M}_{s'}) \end{pmatrix} \begin{pmatrix} \overline{\mathbf{P}}^e \\ \overline{\mathbf{P}}^h \end{pmatrix} \tag{7}$$

$$\overline{\mathbf{E}}_\theta = (E_{\theta,1}, E_{\theta,2}, ..., E_{\theta,N_\theta})^T \tag{8}$$

$$\overline{\mathbf{E}}_\phi = (E_{\phi,1}, E_{\phi,2}, \ldots, E_{\phi,N_\phi})^T \tag{9}$$

where N_θ, N_ϕ are the numbers of measurement points in θ and ϕ directions, respectively. $\overline{\mathbf{E}}_\theta$ and $\overline{\mathbf{E}}_\phi$ are column vectors. Superscript T denotes transpose. The block matrices $\overline{\overline{\mathbf{Z}}}_{\theta,J_{s'}/M_{s'}}$ at the first row of the impedance matrix $\overline{\overline{\mathbf{Z}}}$ represent the contribution to the θ components of the electric field from the equivalent currents. The block matrices $\overline{\overline{\mathbf{Z}}}_{\phi,J_{s'}/M_{s'}}$ at the second row of the impedance matrix $\overline{\overline{\mathbf{Z}}}$ represent the contribution to ϕ components of the electric field from the equivalent currents. Column vectors $\overline{\mathbf{P}}^e$ and $\overline{\mathbf{P}}^h$ are unknown coefficients. Then, conjugate gradient method can be employed to solve the matrix equation in (7).

Since this inverse radiation problem is ill-conditioned, the two normalization factors J_0 and M_0 are introduced to improve the conditioning of the matrix equation system. A better conditioned system can be achieved by choosing J_0 and M_0 according to $M_0/J_0 = \eta_0$, where either M_0 or J_0 can choose freely.

3. ITERATIVE SRM USING PHASELESS FIELD DATA

The aforementioned SRM uses both amplitude and phase information obtained from one measurement surface. It can not work for SRM using amplitude-only data. In this paper, an novel iterative SRM is developed to overcome the absence of the phase information. Instead of requiring both amplitude of phase information, this iterative SRM needs field amplitude over two domains surrounding the DUT/AUT. To simplify the practical measurement procedure, the arbitrary measurement domain is specified to be a spherical surface.

In the first iteration, the measured field amplitude over one spherical surface with an assumed initial phase is employed to facilitate the source reconstruction as indicated in (7). Next, the reconstructed source is applied to calculate the field over another spherical surface while the following error function in (10) is applied to evaluate the accuracy of the reconstructed field.

$$\sigma_{tolerance} = \frac{\| |\mathbf{E}_{SRM}| - |\mathbf{E}_{Meas}| \|}{\|\mathbf{E}_{Meas}\|} \tag{10}$$

where $\mathbf{E}_{SRM}$ is calculated from the reconstructed equivalent current source, and $\mathbf{E}_{Meas}$ is the measured field. If the error is smaller than the pre-defined stop criterion, the iteration will be terminated. Otherwise, the amplitude of the calculated field $\mathbf{E}^{New}$ will be replaced by the measured field amplitude $\|\mathbf{E}^{Meas}\|$ while the phase information is kept. Namely, $||\mathbf{E}_{\theta_l}^{New}||e^{j\theta_l^{New}} \longrightarrow ||\mathbf{E}_{\theta}^{Meas}||e^{j\theta_l^{New}}$, $||\mathbf{E}_{\phi_l}^{New}||e^{j\phi_l^{New}} \longrightarrow ||\mathbf{E}_{\phi}^{Meas}||e^{j\phi_l^{New}}$ after completing the l-th iteration stage.

The next iteration stage repeats the former computation procedure. This iteration process will continue until the pre-defined iteration number is achieved or the error is smaller than the stop criterion. The detailed iteration scheme is presented in Fig. 2.

The iteration scheme in Fig. 2 includes two iteration stages. One

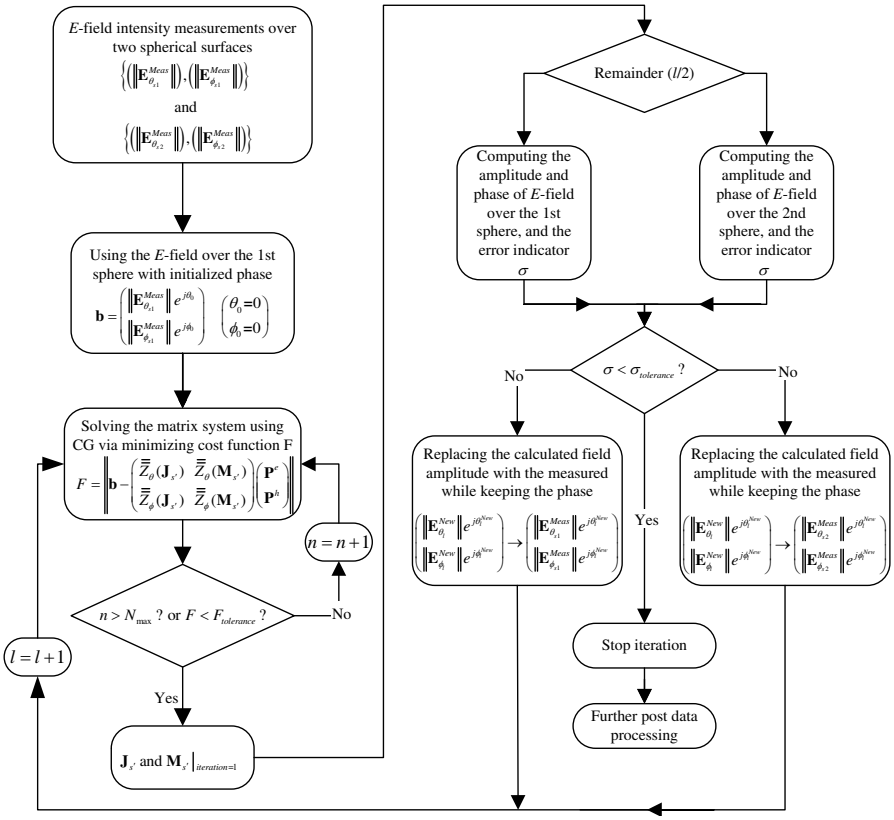

Figure 2. Iteration scheme for the phaseless source reconstruction method.

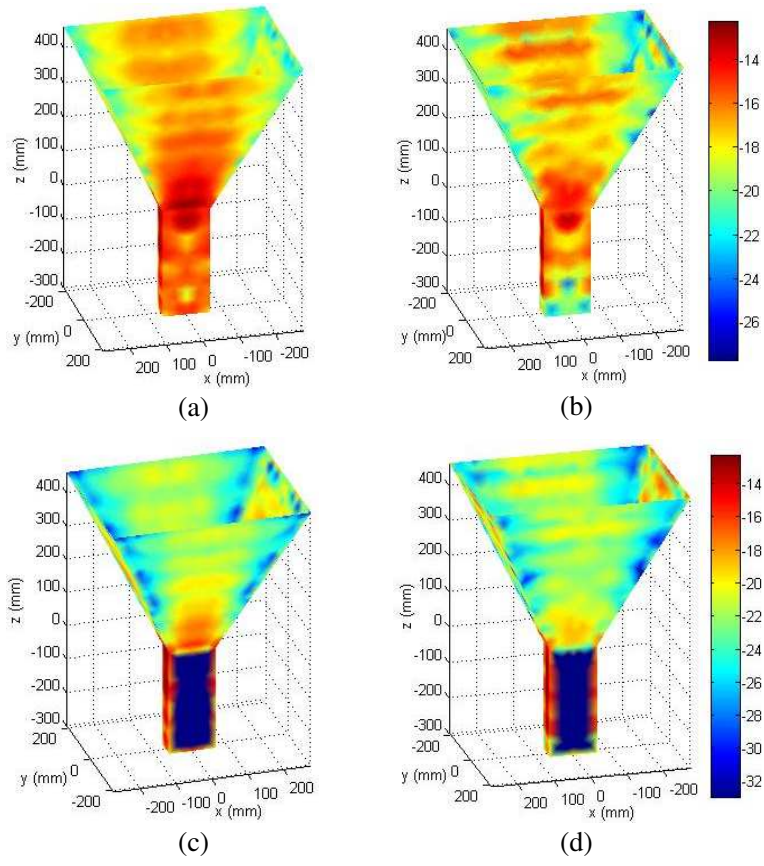

Figure 3. Reconstructed equivalent electric current density (dB A/m^2). Left column is obtained by the conventional SRM using E-field with both amplitude and phase. Right column is obtained by "iterative SRM" using E-field with amplitude-only data. (a)–(b) Total current distribution. (c)–(d) Y components.

is the inner iteration that completes the source reconstruction by solving (7) via the conjugate gradient method. The cost function defined below is minimized in this process.

$$F = \left\| \overline{\mathbf{b}} - \begin{pmatrix} \overline{\overline{\mathbf{Z}}}_\theta(\mathbf{J}_{s'}) & \overline{\overline{\mathbf{Z}}}_\theta(\mathbf{M}_{s'}) \\ \overline{\overline{\mathbf{Z}}}_\phi(\mathbf{J}_{s'}) & \overline{\overline{\mathbf{Z}}}_\phi(\mathbf{M}_{s'}) \end{pmatrix} \begin{pmatrix} \overline{\mathbf{P}}^e \\ \overline{\mathbf{P}}^h \end{pmatrix} \right\| \tag{11}$$

where vector $\mathbf{b}$ in (11) contains both phase and amplitude information

and is expressed as

$$\overline{\mathbf{b}} = \begin{pmatrix} \|\overline{\mathbf{E}}_\theta\|_{Meas} e^{j\theta_{l-1}} \\ \|\overline{\mathbf{E}}_\phi\|_{Meas} e^{j\phi_{l-1}} \end{pmatrix} \tag{12}$$

The element amplitude in $\overline{\mathbf{b}}$ is the measured data. The phase information at $l-1$ stage is calculated using the proposed iterative process.

Another iteration stage is the outer iteration that implements the wave propagation between the source and the next measurement spherical surface. This iteration bridges the relationship between the first and second measurement surfaces.

4. NUMERICAL RESULTS

To verify the accuracy and capability of the "iterative SRM" algorithm, both directive and weakly directive antennas are investigated. For theoretical methodology verification purposes, the sampled field amplitude data is obtained from FEKO [25] full simulations.

4.1. A Rectangular Horn Antenna Operating at L-band

A horn antenna [25] with the aperture size $55 \times 42.8\,\mathrm{cm}^2$ operating at 1.645 GHz is studied first. The measurements are conducted over two spherical surfaces with radii equal to 2 m and 3 m, respectively. To augment the phase variation of the fields between the first and second surfaces, a large separation is preferred. In this case, the separation distance is $d = 1\,\mathrm{m} \approx 5\lambda$, which is large enough to guarantee the phase variation [20]. The angular resolution is $\Delta\theta = \Delta\phi = 5^\circ$.

The equivalent current surface is chosen to fit the physical surface of the horn antenna. This surface is triangulated into 1848 patches. Only electric current is needed since the current resides only over the PEC surface of this horn antenna. The electric current is represented by 2738 RWG basis functions.

The matrix equation thereby has 5184 equations and 2738 unknowns. It is solved through the conjugate gradient method minimizing the residue norm in (11).

The reconstructed equivalent current by the proposed phaseless "iterative SRM" is shown in Figs. 3(b), (d). For comparison, its counterpart reconstructed from both amplitude and phase information sampled over a spherical surface with radius 2 m is shown in Figs. 3(a), (c). Good agreement is obtained. The difference observed in (a) and (b) is due to the existence of null space of the inverse problem. The reconstructed source is polluted by non-radiating currents.

To show the effectiveness of far field calculation, the reconstructed far field pattern by our method is shown in Fig. 4 with the simulated data from FEKO. Good agreements are achieved. To further explain the effectiveness of our method, the reconstructed phase information is presented in Fig. 5. The missing of phase information makes the phase prediction poor than those with both phase and amplitude information.

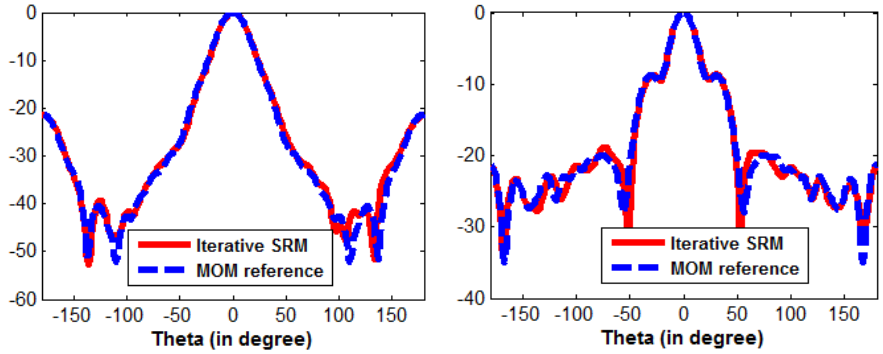

Figure 4. The reconstructed far field pattern (in dB) using amplitude-only data. (a) Far field pattern in the XOZ plane. (b) Far field pattern in the YOZ plane.

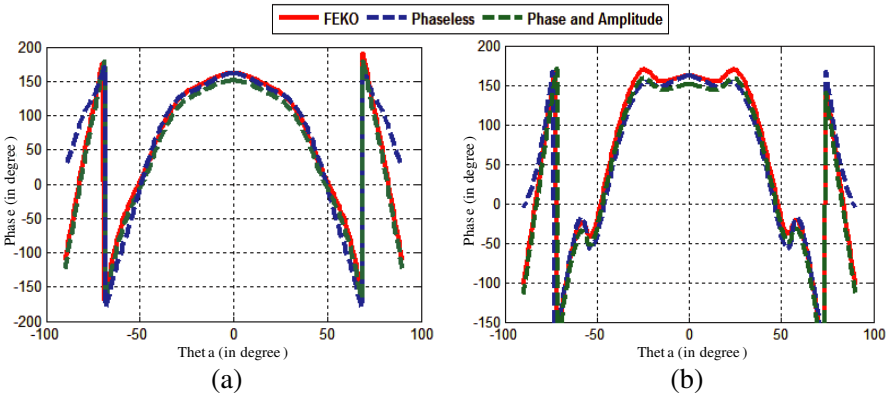

Figure 5. The reconstructed phase information of the field in (a) the XOZ plane and (b) the YOZ plane.

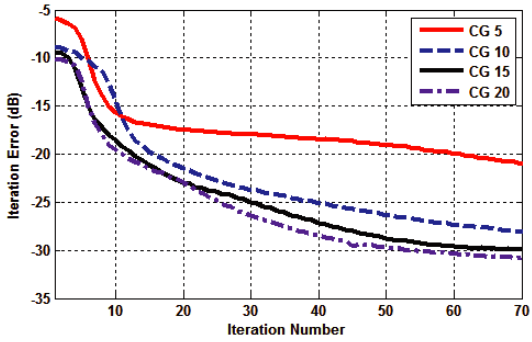

Figure 6. The convergence rate of the phaseless SRM using different iteration number at the CG stage.

4.2. A Coaxially-fed Rectangular Microstrip Patch Antenna

In this example, a microstrip patch antenna [25] is employed to investigate the feasibility of the iterative SRM for characterizing weakly directional and medium gain antennas. The patch antenna works at 3 GHz. Its 2D dimension is $46.8 \times 33.2\,\text{mm}^2$ and the corresponding border between the Fresnel region and Fraunhofer region is at $R \approx 1.15\,\text{m}$. The electric field amplitude measurement is conducted over two spherical surfaces with radii $R = 1\,\text{m}$ and $R = 2\,\text{m}$, respectively. The separation between them is 10λ that is sufficiently larger to ensure the phase diversification. The angular steps are $\Delta\theta = \Delta\phi = 5^\circ$.

The patch antenna consists of two kinds of material: dielectric and PEC. Hence, two different boundary conditions must be enforced. First, the electric current exists at both dielectric and PEC regions since the tangential magnetic field is non-zero. Secondly, the tangential electric field is zero over the PEC region. Therefore, the magnetic current only exists at dielectric region. To model the equivalent electric current, the whole patch surface is discretized into 1684 triangle patches, resulting 2526 unknowns. As for the magnetic current, only the dielectric region is discretized, resulting 666 triangles and 930 unknowns. The final matrix system involves 5184 equations and 3456 unknowns, which is solved by the conjugate gradient method in the iterative SRM. To study the effect of the number of iteration at the CG stage on the convergence rate, the results according to the different iteration numbers of CG are shown in Fig. 6. It is noted that the convergence speed will not increase with the CG iteration number. The iteration number from 10 to 20 is enough.

The reconstructed electric and magnetic currents are shown in

Fig. 7 and Fig. 8, respectively. In Fig. 7, the current in the center is very strong which complies with the physical current distribution since that region is the PEC where the feeding point locates. Since the current has only tangential component, the z-component should

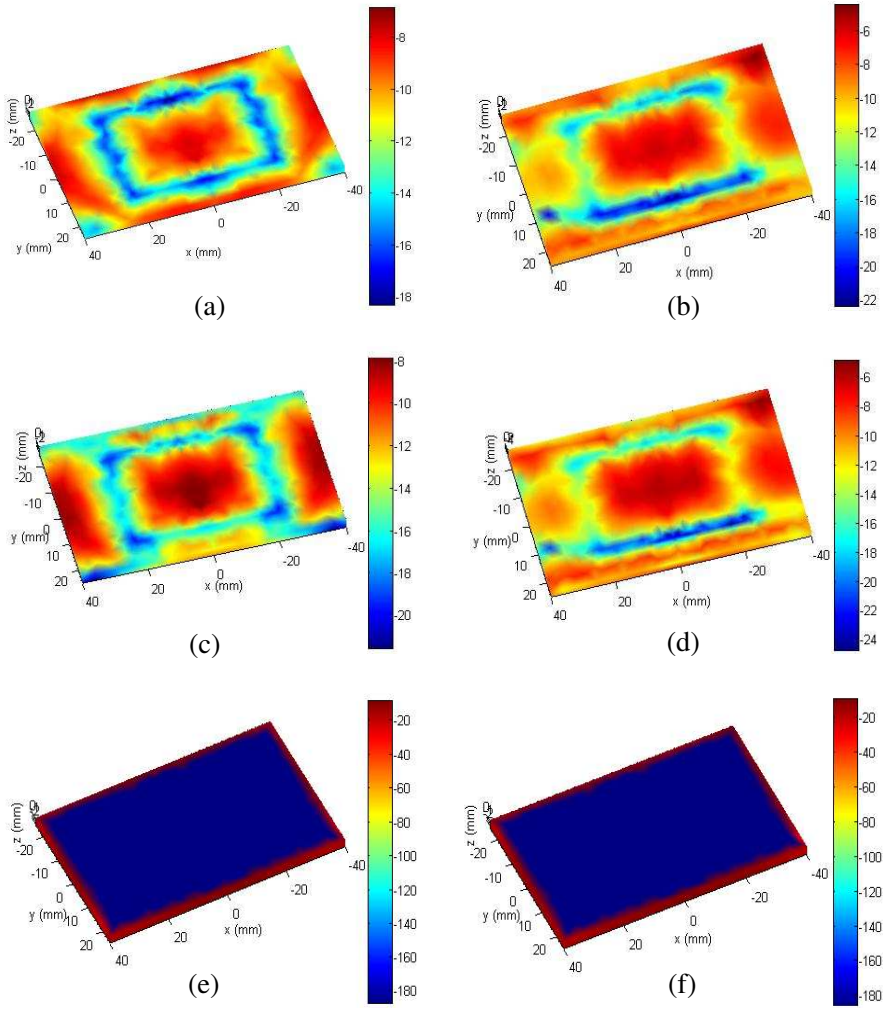

Figure 7. Reconstructed equivalent electric current density (dB A/m^2). Left column is obtained by the conventional SRM using E-field with both amplitude and phase. Right column is obtained by "Iterative-SRM" using E-field with amplitude-only data. (a)–(b) Total current distribution. (c)–(d) Y components. (e)–(f) Z components.

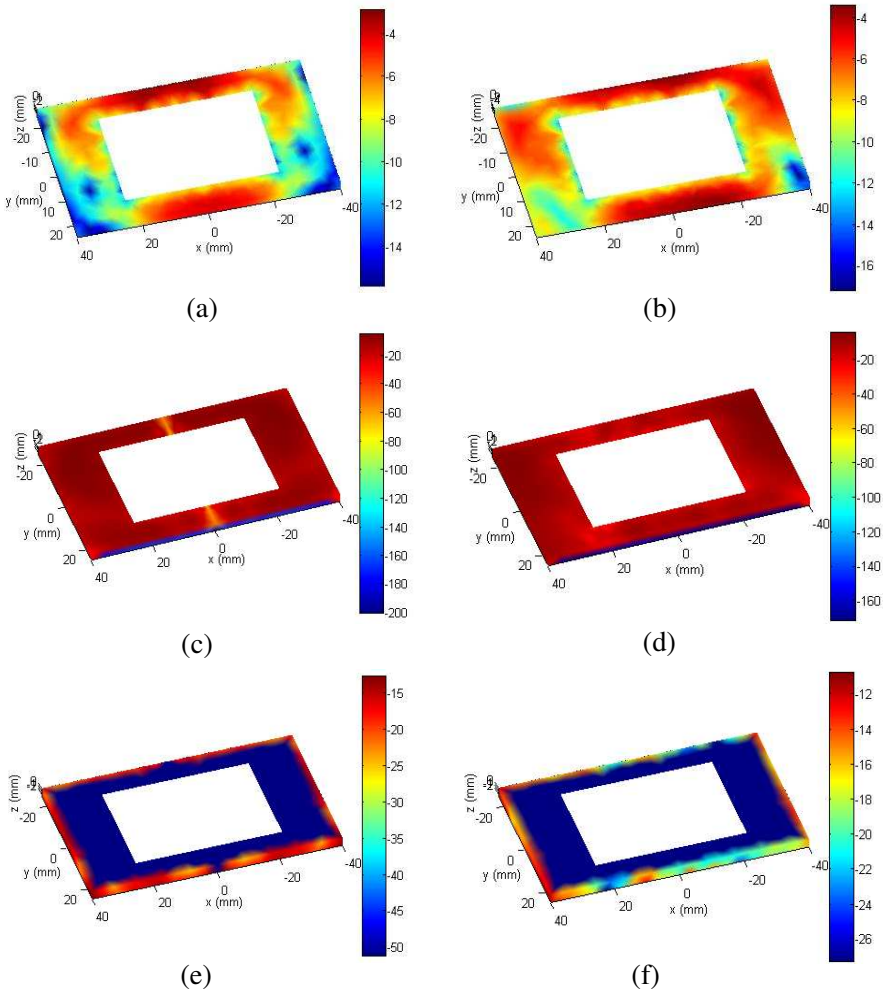

Figure 8. Reconstructed equivalent magnetic current density (dB A/m^2). Left column is obtained by conventional SRM using E-field with both amplitude and phase; right column is obtained by "iterative SRM" using E-field with amplitude-only data. (a)–(b) Total current distribution. (c)–(d) Y components. (e)-(f) Z components.

be zero in the horizontal plane. For the magnetic current distribution, the strong current should exist along the edges due to the discontinuity. The resultant currents in Fig. 8 also comply with this statement. Also, the differences are attributed to the existence of non-radiating sources. Next, the predicted far field pattern calculated from the reconstructed

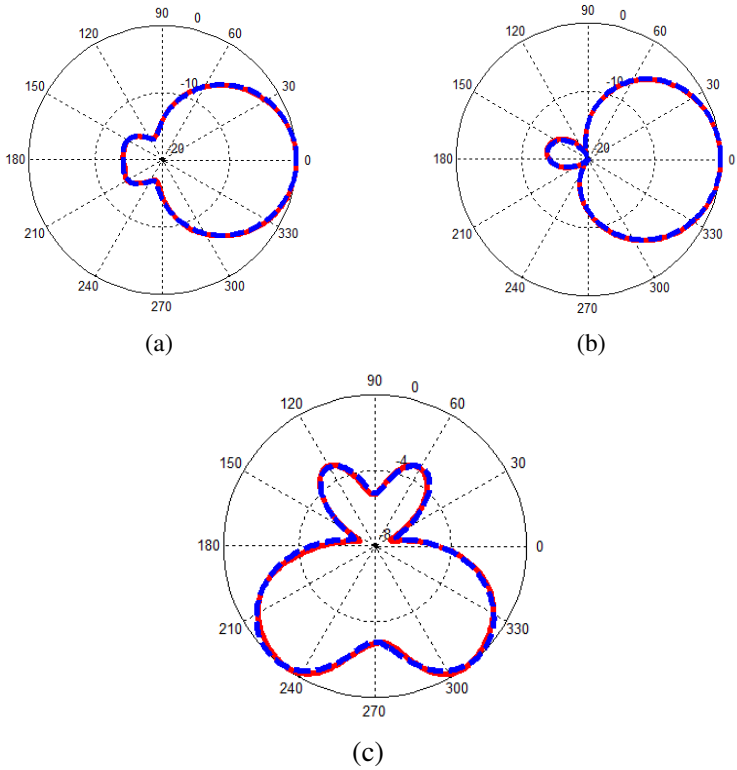

Figure 9. The reconstructed far field pattern (in dB) using the amplitude-only data for the patch antenna. (a) Far field pattern in the XOZ plane. (b) Far field pattern in the YOZ plane. (c) Far field pattern in the XOY plane.

equivalent current source is shown in Fig. 9. The results are compared with the reference data obtained from FEKO. Excellent agreements are achieved.

To have a quantitative understanding of the precision of the proposed iterative SRM using the amplitude-only information, the field intensity over a spherical surface with radius equal to 2 m is calculated from the reconstructed current source as shown in Fig. 10, the reconstructed field agrees with that from FEKO very well. The error indicator in (10) versus the different radius of the observation spherical surfaces is shown in Fig. 11. It is observed that the SRM using both phase and amplitude information is more accurate than the phaseless SRM. Also, the accuracy in the near-field region is poor than that in the far-field region. The reason for this phenomenon is due to

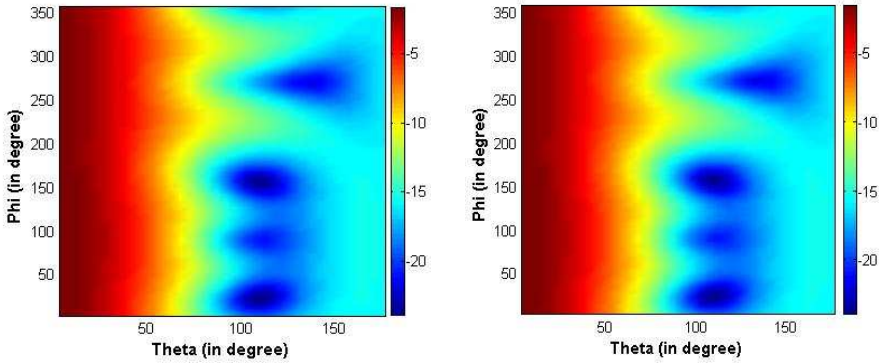

Figure 10. Amplitude of electric field (in dB) over a spherical surface with radius equal to 2 m. (a) Calculated from the equivalent current source using amplitude-only data. (b) Calculated from the full wave simulation by FEKO.

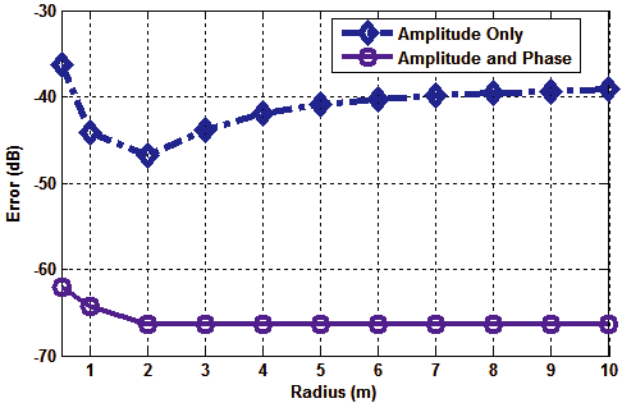

Figure 11. The error function (in dB) in (10) versus the observation distance (m).

the existence of evanescent waves in the near-field region, which is hard to capture.

We observe that the presented technique is very similar to the alternating-projection approach used in different fields and especially in pattern synthesis [17, 18].

5. CONCLUSION

A novel phaseless iteration SRM in a forward-backward fashion is presented. The equivalent current source residing on the surface of the antenna is reconstructed using amplitude-only measurements. Both highly directive and weakly directive antenna are benchmarked and very good agreements are achieved. Meanwhile, the 3D radiation pattern can be thoroughly characterized. Due to its high accuracy and versatile, this phaseless iteration SRM is of particular interest for situations where only the magnitude measurements is possible. However, the stability of the proposed method needs further study since no real measurement data including noise is used.

ACKNOWLEDGMENT

We thank Professor W. C. Chew for his constructive suggestions. Also, this work was supported in part by the Research Grants Council of Hong Kong (GRF 711511 and 713011), HKU Small Project Funding (201007176196), and in part by the University Grants Council of Hong Kong (Contract No. AoE/P-04/08).

REFERENCES

1. Laurin, J. J., J. F. Zurcher, and F. Gardiol, "Near-field diagnostics of small printed antennas using the equivalent magnetic current approach," *IEEE Trans. Antennas Propag.*, Vol. 49, No. 5, 814–828, May 2001.
2. Donelli, M., S. Caorsi, F. De Natale, D. Franceschini, and A. Massa, "A versatile enhanced genetic algorithm for planar array design," *Journal of Electromagnetic Waves and Applications*, Vol. 18, No. 11, 1533–1548, 2006.
3. Donelli, M., R. Azaro, F. D. Natale, E. Zeni, and A. Massa, "Optimized design of a multifunction/multiband antenna for automotive rescue systems," *IEEE Trans. Antennas Propag.*, Vol. 54, No. 2, 392–400, 2006.
4. Donelli, M., R. Azaro, L. Fimognari, R. Azaro, and A. Massa, "A planar electronically reconfigurable Si-Fi band anntenna based on parasitic microstrip structure," *IEEE Antennas Wireless Propag. Lett.*, No. 6, 623–626, 2007.
5. Weng, H., D. Beetner, R. E. Dubroff, and J. Shi, "Estimation of high frequency currents from the near-field scan measurement," *IEEE Trans. Electromagn. Compat.*, Vol. 49, No. 4, Nov. 2007.

6. Peter, P. and T. K. Sarkar, "Planar near-field to far-field transformation using an equivalent magnetic current approach," *IEEE Trans. Antennas Propag.*, Vol. 40, No. 11, 1348–1356, Nov. 1992.
7. Taaghol, A. and T. K. Sarkar, "Near-field to near/far-field transformation for arbitrary near-field geometry, utilizing an equivalent magnetic current," *IEEE Trans. Antennas Propag.*, Vol. 38, No. 3, 536–542, Aug. 1996.
8. Sarkar, T. K. and A. Taaghol, "Near-field to near/far-field transformation for arbitrary near-field geometry utilizing an equivalent electric current and MOM," *IEEE Trans. Antennas Propag.*, Vol. 47, No. 3, 566–573, Mar. 1999.
9. Alvarez, Y., F. Las-Heras, and M. R. Pino, "Reconstruction of equivalent currents distribution over arbitrary three-dimensional surfaces based on integral equation algorithms," *IEEE Trans. Antennas Propag.*, Vol. 55, No. 12, 3460–3468, Nov. 2007.
10. Alvarez, Y., F. Las-Heras, M. R. Pino, and T. K. Sarkar, "An improved super-resolution source reconstruction method," *IEEE Trans. Antennas Propag.*, Vol. 58, No. 11, 3855–3866, Nov. 2009.
11. Serhir, M., P. Besnier, and M. Drissim, "An accurate equivalent behavioral model of antenna radiation using a mode-matching technique based on spherical near field measurements," *IEEE Trans. Antennas Propag.*, Vol. 56, No. 1, 48–57, Jan. 2008.
12. Persson, K. and M. Gustafsson, "Reconstruction of equivalent currents using a near-field data transformation-with radome applications," *Progress In Electromagnetics Research*, Vol. 54, 179–198, 2005.
13. Quijano, J. L. A. and G. Vecchi, "Improved-accuracy source reconstruction on arbitrary 3-D surfaces," *IEEE Antennas Wireless Propag. Lett.*, Vol. 8, 1046–1049, Sep. 2009.
14. Eibert, T. F. and C. H. Schmidt, "Multilevel fast multipole accelerated inverse equivalent current method employing Rao-Wilton-Glisson discretization of electric and magnetic surface currents," *IEEE Trans. Antennas Propag.*, Vol. 57, No. 4, 1178–1185, 2009.
15. Eibert, T. F., Ismatullah, E. Kaliyaperumal, and C. H. Schmidt, "Inverse equivalent surface current method with hierarchical higher order basis functions, full probe correction and multilevel fast multipole acceleration," *Progress In Electromagnetics Research*, Vol. 106, 377–394, 2010.
16. Jorgensen, E., P. Meincke, and M. Sabbadini, "Improved source reconstruction technique for antenna diagnostics," *Proc. 32nd*

ESA Antenna Workshop, Nordwijk, The Netherlands, Oct. 2010.

17. Bucci, O. M., G. Franceschetti, G. Mazzarella, and G. Panariello, "Intersection approach to array pattern synthesis," *IEEE Proceedings H Microw. Antennas Propag.*, Vol. 82, No. 3, 349–357, Dec. 1990.
18. Bucci, O. M., G. D. Elia, G. Mazzarella, and G. Panariello, "Antenna pattern synthesis: A new general approach," *Proceedings of IEEE*, Vol. 82, No. 3, 358–371, Mar. 1994.
19. Las-Heras, F. and T. K. Sarkar, "A direct optimization approach for source reconstruction and NF-FF transformation using amplitude-only data," *IEEE Trans. Antennas Propag.*, Vol. 50, No. 4, 500–510, Aug. 2002.
20. Schmidt, C. H., S. F. Razavi, T. F. Eibert, and Y. Rahmat-Samii, "Phaseless spherical near-field antenna measurements for low and medium gain antennas," *Adv. Radio Sci.*, Vol. 8, 43–48, 2010.
21. Alvarez, Y., F. Las-Heras, and M. R. Pino, "The sources reconstruction method for amplitude-only field measurements," *IEEE Trans. Antennas Propag.*, Vol. 58, No. 8, 2776–2781, Aug. 2010.
22. Rengarajan, S. R. and Y. Rahmat-Samii, "The field equivalence principle: Illustration of the establishment of the non-intuitive null fields," *IEEE Trans. Antennas Propag.*, Vol. 42, No. 4, 122–128, Aug. 2000.
23. Quijano, J. L. A. and G. Vecchi, "Field and source equivalence in source resconstruction on 3D surfaces," *Progress In Electromagnetics Research*, Vol. 103, 67–100, 2010.
24. Rao, S. M., D. R. Wilton, and A. W. Glisson, "Electromagnetic scattering by surfaces of arbitrary shape," *IEEE Trans. Antennas Propag.*, Vol. 30, No. 3, 409–418, May 1982.
25. EM Software and Systems, FEKO Suite 6.0 [Online]. Available: http:// www.feko.info.
26. Quijano, J. L. A. and G. Vecchi, "Near- and very near-field accuracy in 3-D source reconstruction," *IEEE Antennas Wireless Propag. Lett.*, Vol. 9, 634–637, 2010.
27. Quijano, J. L. A., L. Scialacqua, J. Zackrisson, L. J. Foged, M. Sabbadini, and G. Vecchi, "Suppression of undesired radiated fields based on equivalent currents reconstruction from measured data," *IEEE Antennas Wireless Propag. Lett.*, Vol. 10, 314–317, 2011.